




Manufacturing Technologies and Applications

MATECA



Investigation on Weldability and Post-Weld Heat Treatment of A 333 Gr.6 and A350LF-2 Steels

Esin Tuğba Şimşek Çelik^{1,*} , Başar Ersegün Çelik² , Şükrü Talaş¹ 

¹Sivas Cumhuriyet University, Hafik Kamer Ornek Vocational School of Higher Education, Department of Transportation Services, Rail Systems Management Program, Sivas, Türkiye

²Afyon Kocatepe University, Institute of Natural Sciences, Afyonkarahisar, Türkiye

¹Department of Metallurgical and Materials Engineering, Faculty of Technology, Afyon Kocatepe University, Afyonkarahisar, Türkiye

ABSTRACT

In this study, as the first welding process, GTAW (Gas Tungsten Arc Welding) welding process was carried out on 9.53 mm thick A 333 Gr.6 pipe and A350LF-2 flange steels using 2.4 mm ER70S-6 electrode and SMAW (Manual Arc Welding) welding process was carried out using 2.5 mm E 7018-1 electrode for filler and cover passes. As the second welding process, GTAW welding process was carried out on 5.49 mm thick A 333 Gr.6 pipe and A350LF-2 flange steels using 2.4 mm ER70S-6 electrode and SMAW welding process was carried out using 2.5 mm E 7018-1 electrode for filler and cover passes. Post-weld heat treatment was applied during the first welding process. No post-weld heat treatment was applied during the second welding process. The effect of heat treatment on some mechanical properties of the materials and the changes that occur after stress relief were investigated for the welds made with the same materials, the same electrodes, the same welding methods but with different thicknesses. Tensile test, bending test, hardness test, notch impact test was performed as mechanical tests of the welded parts, macro images were taken and comparisons were made. As a result, the effects on the weld quality were investigated and results indicate that welding processes were successfully carried out with given filler electrodes and steel pipes.

Keywords: A 333 Gr.6, A350LF-2, GTAW, SMAW

A 333 Gr.6 ile A350LF-2 Çeliklerinin Kaynaklanabilirliğinin ve Kaynak Sonrası Isıl İşlemlerinin İncelenmesi

ÖZET

Bu çalışmada ilk kaynak işlemi olarak, 9.53 mm kalınlığında A 333 Gr.6 boru ile A350LF-2 flanş çeliklerinin GTAW (Gaz Tungsten Ark Kaynağı) kaynak işlemi 2,4 mm ER70S-6 elektrodu kullanılarak, SMAW (Manuel Ark Kaynağı) kaynak işlemi ise dolgu ve kapak pasoları için 2,5 mm E 7018-1 elektrodu kullanılarak gerçekleştirilmiştir. İkinci kaynak işlemi olarak, 5.49 mm kalınlığında A 333 Gr.6 boru ile A350LF-2 flanş çeliklerinin GTAW kaynak işlemi 2,4 mm ER70S-6 elektrodu kullanılarak, SMAW kaynak işlemi ise dolgu ve kapak pasoları için 2,5 mm E 7018-1 elektrodu kullanılarak gerçekleştirilmiştir. İlk kaynak işlemi gerçekleştirilirken kaynak sonrası ısıtım uygulanmıştır. İkinci kaynak işlemi gerçekleştirilirken kaynak sonrası ısıtım uygulanmamıştır. Aynı malzemelerle, aynı elektrotlarla, aynı kaynak yöntemleriyle ama farklı kalınlıklarda gerçekleştirilen kaynaklara ısıtım uygulamanın malzemelerin bazı mekanik özelliklerine olan etkisi ve gerilme giderme sonrası meydana gelen değişiklikler incelenmiştir. Elde edilen kaynaklı parçaların mekanik testleri olarak çekme testi, eğme testi, sertlik testi, çentik darbe testi gerçekleştirilmiş, makro görüntüleri çekilmiş, karşılaştırılmaları yapılmıştır. Sonuç olarak kaynak kalitesi üzerindeki etkiler araştırılmış ve sonuçlar verilen dolgu elektrotları ve çelik borularla kaynak işlemlerinin başarıyla gerçekleştirildiğini göstermektedir.

Anahtar Kelimeler: A 333 Gr.6, A350LF-2, GTAW, SMAW

1. INTRODUCTION

Pipes are widely produced and utilized in large quantities globally, particularly in heavy industries such as offshore transportation and oil extraction [3]. Pipelines in offshore platforms are constructed from a range of materials, selected based on factors such as cost, functional requirements, operating conditions (pressure and temperature), and corrosion rate, among others [1, 2]. This widespread use is attributed to low carbon steels due to their high strength, excellent weldability, resistance to high temperatures, and effective surface protection against environmental factors. Additionally, it is more cost-effective compared to other alloy

*Corresponding author, e-mail: esimsek@cumhuriyet.edu.tr

steels like low alloy steel and especially stainless steel [4, 5]. In the pipeline industry, medium and high carbon steels are generally avoided due to their increased brittleness and reduced weldability, particularly for offshore applications [6]. As a result, low carbon steel is preferred for offshore pipelines among designers, fabricators, and regulators. It is commonly used in the construction of pipelines for high-temperature vessels, heat exchangers, compressors, and transmission lines [6, 7]. A333 Grade 6 pipe, in particular, is referred to as a low-temperature pipe because it can withstand impacts to produce ductile failure at temperatures as low as -45°C [8]. ASTM A333 Gr.6 and ASTM A350 LF-2 are commonly used in environments with temperatures as low as -50°C . The primary challenge in welding these materials is ensuring that they maintain toughness at such low temperatures. Although low-temperature carbon steel typically exhibits good toughness and plasticity, the reheating process during welding can cause grain growth, which leads to a reduction in both toughness and plasticity. Therefore, using the appropriate welding process, consumables, parameters, and carefully controlling heat input are crucial to meet the required toughness in low-temperature conditions [9]. ASTM A350 LF-2 is low-strength and relatively cost-effective, known for their excellent weldability. This is largely due to the absence of elements, such as chromium (Cr), nickel (Ni), and molybdenum (Mo), which makes them easier to weld [10].

In the study by Wang & Chang [9], automatic and high-efficiency TIG (Tungsten Inert Gas) welding was applied for root and hot welding of ASTM A333 Gr.6 (low-temperature carbon steel, designed for -50°C) and ASTM A312/A358 TP304/304L (austenitic stainless steel, designed for -196°C) pipes. The study explored the design of the welding process, welding parameters, and tests and analyses of the mechanical properties of the welds, focusing on the advantages of automatic TIG welding. The results showed that automatic TIG welding improved efficiency by twofold compared to traditional manual TIG welding, leading to enhanced quality in process piping. In the study by Nissan & Baker [10], six ASTM A350 LF2 flanges exhibited a wide variation in low-temperature (-50°F) Charpy impact toughness, with values ranging from as low as 4 J to over 298 J. These flanges, characterized by relatively low strength with minimum yield strength of 248 MPa and tensile strength between 483 and 655 MPa, had similar yield and ultimate tensile strengths (UTS), despite the significant differences in toughness values. A detailed chemical and microstructural analysis was conducted to investigate the cause of this variability. Most of the flanges contained aluminium and had a fine grain structure, with the toughness variation largely attributed to the cooling rate after normalizing. Flanges cooled in still air showed the lowest toughness, while those forced air cooled exhibited the highest toughness. For flanges at this strength level, a quench and temper process is not required to achieve good low-temperature toughness; however, a minimum cooling rate, such as forced air cooling after normalizing, is necessary to ensure both good toughness and overall strength. In the study by Ghosh et al. [11], weld joints of SA 333 Gr. 6 steel pipes were prepared using a GTAW root pass and a V-groove SMAW filler. The objective was to characterize the base metal, weld deposit, and heat-affected zone (HAZ) of the pipe weld in terms of their chemical composition, metallurgical structure, mechanical properties, and fracture mechanics. The fracture toughness of the welds and HAZ was evaluated using J-integral parameters. Additionally, the fracture mechanics properties of the base metal, weld, and HAZ were compared and correlated, with a further correlation drawn between the fracture mechanics properties of the weld and HAZ and their respective microstructures. In the study by Efzan et al. [12], the microstructure of A333 Grade 6 steel pipe was analysed using light microscopy to characterize the material's structure. A hardness test was also performed to assess the material's resistance to applied force. The study concluded that A333 Grade 6 low-carbon steel has a microstructure with smaller grain size and lower pearlite content, which supports its high strength and ductility. The average hardness value measured for the steel was 166.836 HV, well within the acceptable range for oil and gas pipelines, where the maximum hardness allowed is 250 HV. Given its hardness level, A333 Grade 6 steel is well-suited for use in offshore platform pipelines.

In this study, as the first welding process, GTAW welding process was carried out on 9.53 mm thick A 333 Gr.6 pipe and A350LF-2 flange steels using 2.4 mm ER70S-6 electrode and SMAW welding process was carried out using 2.5 mm E 7018-1 electrode. As the second welding process, GTAW welding process was carried out on 5.49 mm thick A 333 Gr.6 pipe and A350LF-2 flange steels using 2.4 mm ER70S-6 electrode and SMAW welding process was carried out using 2.5 mm E 7018-1 electrode. Post-weld heat treatment was applied during the first welding process. No post-weld heat treatment was applied during the second welding process. The effect of heat treatment on some mechanical properties of the materials and the changes that occur after stress relief were investigated for welds made with the same materials, the same electrodes, the same welding methods but with different thicknesses. Tensile, bending, hardness, notch impact tests were performed as mechanical tests on the welded parts, macro images were taken and comparisons were made to observe the effects on the weld quality.

2. MATERIAL AND METHOD

2.1. Experimental Studies

In this study, GTAW (Gas Tungsten Arc Welding) welding process was carried out on 9.53 mm thick A 333 Gr.6 pipe and A350LF-2 flange steels using 2.4 mm ER70S-6 electrode as the first welding process and SMAW (Manual Arc Welding) welding process was carried out using 2.5 mm E 7018-1 electrode for filler and cover passes. The first welding process was given the code W-A; the properties of base metals, welding electrodes, welding methods and position of welding passes used in the W-A coded welding process are shown in Figure 1. The chemical composition of the A 333 Gr.6 steel is given in Table 1, the chemical composition of the A350LF-2 flange steel is given in Table 2, the chemical composition of the ER70S-6 electrode is given in Table 3, and the chemical composition of the E 7018-1 electrode is given in Table 4.

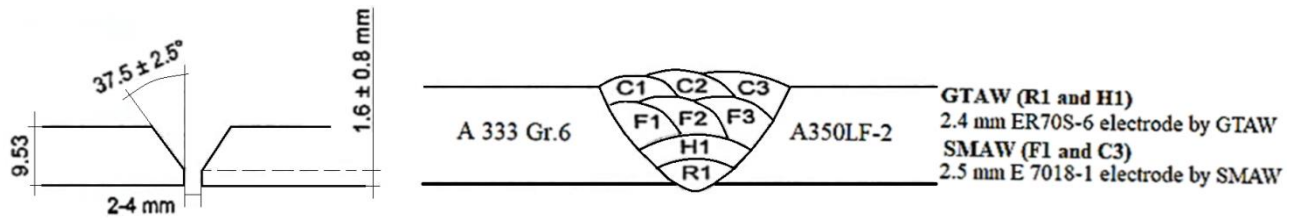


Figure 1. Weld groove, base metals, welding electrodes, welding methods and welding passes used in the W-A coded welding process

Table 1. Chemical composition of A 333 Gr.6 steel (wt. %)

C	Si	Mn	Cr	Mo	P	S	Ni	V	Al	Sn	Cu	Nb	Ti
0.11	0.24	1.05	0.03	0.06	0.012	0.001	0.038	0.037	0.028	0.009	0.069	0.002	0.012

Table 2. Chemical composition of A350LF-2 steel (wt. %)

C	Si	Mn	P	S	Cr	Ni	Mo	Nb	V	Cu	Al
0.200	0.280	0.840	0.008	0.001	0.090	0.090	0.040	0.005	0.003	0.280	0.030

Table 3. Chemical composition of ER70S-6 electrode (wt. %)

C	Si	Mn	P	S	Cr	Ni	Mo	Cu	V	Al	Ti+Zr
0.08	0.86	1.60	0.013	0.008	0.03	0.01	<0.01	0.05	<0.01	<0.01	0.01

Table 4. Chemical composition of E 7018-1 electrode (wt. %)

C	Si	Mn	P	S	Cr	Ni	Mo	Nb	Cu	V
0.06	0.59	1.59	0.022	0.007	0.05	0.02	0.01	0.01	0.03	0.02

In the W-A coded welding process, a total of 8 passes were applied, including 1 root pass, 1 hot pass, 3 filler passes, and 3 cover passes. The root pass and hot pass were made with the GTAW method, and the filler passes and cover passes were made with the SMAW method. In the W-A coded welding process, the welding passes, welding current and voltage, welding travel speed, and total heat input values are given in Table 5.

In the W-A coded welding process, the preheating temperature was 100 °C. The temperature between passes is 250 °C. The post-weld heat treatment (PWHT) temperature was 620 °C and applied for 60 minutes. The heating rate and cooling rate were kept constant at 180 °C/h. The thermal cycle and PWHT of the W-A coded welding process are given in Figure 2.

In this study, as the second welding process, GTAW welding process was performed using 2.4 mm ER70S-6 electrode and SMAW welding process was performed using 2.5 mm E 7018-1 electrode on 5.49 mm thick A 333 Gr.6 and A350LF-2 pipe flange. The second welding process was given the code of W-B. The base metals, electrode types, welding methods and welding passes used in the W-B coded welding process are shown in Figure 3.

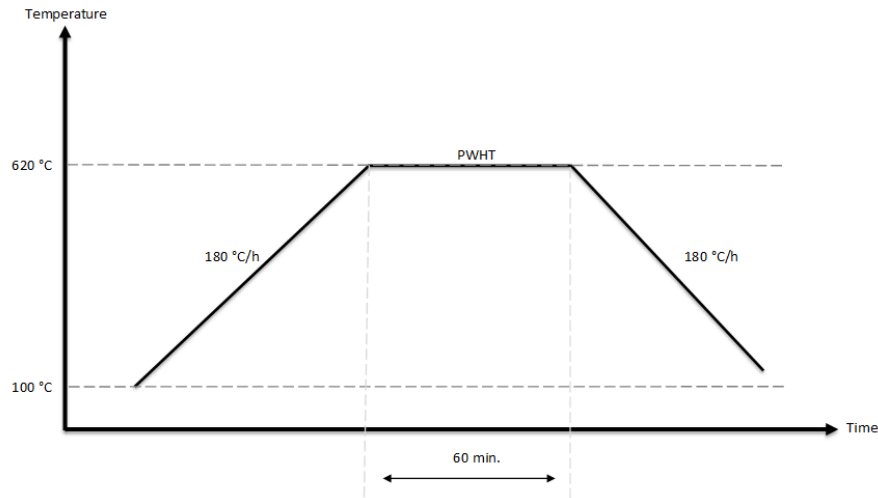


Figure 2. The thermal cycle and PWHT of the W-A coded welding process.

Table 5. Welding passes, welding current, welding voltage, welding travel speed and total heat input values in the W-A coded welding process.

Weld layers	Process	Class	Dia (mm)	Polarity	Amper range	Voltage range	Travel Speed (mm/min)	Heat input (KJ/mm)	Interpass Temp. (°C)
Root	GTAW	ER 70S-6	2.4	DCEN	102	10	41.18	1.49	100
Hot	GTAW	ER 70S-6	2.4	DCEN	162	10	56.63	1.72	185
Fill	SMAW	E 7018-1	2.5	DCEP	83	26	69.51	1.86	190
Fill	SMAW	E 7018-1	2.5	DCEP	90	26	74.32	1.89	190
Fill	SMAW	E 7018-1	2.5	DCEP	95	28	85.19	1.87	185
Cover	SMAW	E 7018-1	2.5	DCEP	91	28	82.30	1.86	200
Cover	SMAW	E 7018-1	2.5	DCEP	93	25	98.39	1.42	180
Cover	SMAW	E 7018-1	2.5	DCEP	92	25	102.15	1.35	200

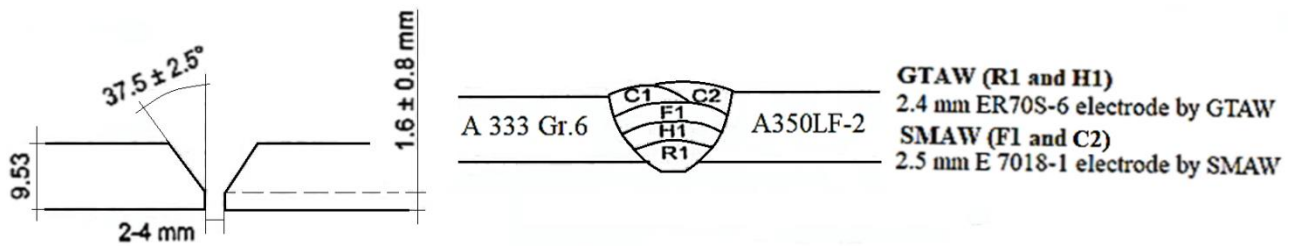


Figure 3. Weld groove, base metals, electrode types, welding methods and welding passes used in the W-B coded welding process.

In the W-B coded welding process, 5 welding passes were applied, including 1 root pass, 1 hot pass, 1 fill pass, and 2 cover passes. The root pass and hot pass were made with the GTAW method, and the fill and cover passes were made with the SMAW method. In the W-B coded welding process, the welding passes, welding current, welding voltage, interpass temperature, welding travel speed, and total heat input values are given in Table 6. In the W-B coded welding process, the preheating temperature is 100 °C. The temperature between weld passes is 185 °C. Heat treatment was not performed after welding. In this study, pure Argon gas was used as a shielding gas during GTAW welding with a gas flow rate of 12-15 lt/min.

Table 6. Welding passes, welding current, welding voltage, welding travel speed and total heat input values in the W-B coded welding process.

Weld layers	Process	Class	Dia (mm)	Polarity	Amper range	Voltage range	Travel Speed (mm/min)	Heat input (KJ/mm)	Interpass Temp. (°C)
Root	GTAW	ER 70S-6	2.4	DCEN	100	11	66.97	0.99	100
Hot	GTAW	ER 70S-6	2.4	DCEN	135	11	118.00	0.76	175
Fill	SMAW	E 7018-1	2.5	DCEP	90	26	105.30	1.33	185
Cover	SMAW	E 7018-1	2.5	DCEP	82	26	130.04	0.98	180
Cover	SMAW	E 7018-1	2.5	DCEP	82	26	122.00	1.05	185

2.2. Mechanical Tests Applied to Welded Parts

Tensile, bending, Charpy V notch impact and hardness tests were performed on welded parts. The hardness tests were carried out using Qness brand hardness tester device with a setting of HV10 and 15s dwelling time. Instron-5989 was used as the tensile test device with a cross-head speed of 3 mm/min. In the bending tests, 4 bending samples (BT) from each of the welds coded W-A and W-B were used. Charpy V notch impact test was performed using Instron (450 J) device. The parameters and conditions employed in the bending tests are given in Table 7.

Table 7. Parameters and conditions used in the bending test of W-A and W-B coded welded samples.

Specimen No	Type of Bend	Position (Deg)	Dimension (mm)	Bend Angle (°)	Former Dia. (mm)
W-A-BT-1	Face Bend	45	38	180	38
W-A-BT-2	Face Bend	225	38	180	38
W-A-BT-3	Root Bend	135	38	180	38
W-A-BT-4	Root Bend	315	38	180	38
W-B-BT-1	Face Bend	45	38	180	4t
W-B-BT-2	Face Bend	225	38	180	4t
W-B-BT-3	Root Bend	135	38	180	4t
W-B-BT-4	Root Bend	315	38	180	4t

3. RESULTS and DISCUSSION

3.1. Tensile Test and Bending Test Results

A 3-point 180° bending test was applied to the test piece samples. The samples showed successful performance in the 180° bending test without tearing, and visible discontinuity or defect was not detected on the test specimens. The successful results of the samples that were bent to 180° three-point bending test show that the welding process was carried out correctly and the selected filler metals were suitable for material combination selected for this process. It is important to note that weld metals are prone to lower fatigue performances due to any flaw at the root welds and this may lead to the structural damage in welds such as friction stir welding [14, 15]. Nevertheless, it has been demonstrated that root welds exhibit lower levels of stress in relation to fatigue failure when compared with cover welds. This is attributable to the divergent stress directions exhibited by these welds, whereby root welds are subject to compression stress, whilst cover welds experience tensile stress [14]. Tensile test results on samples (TT) obtained from the welding processes coded W-A and W-B are given in Table 8. The tensile test results graph is given in Figure 4.

Table 8. Tensile test results on samples obtained from the welding process coded W-A and W-B (UTS: Ultimate Tensile Stress, UTL: Ultimate Total Load, YS: Yield Strength)

Specimen No	Dimension (mm)	Area (mm ²)	UTL (KN)	YS (MPa)	UTS (N/mm ²)
W-A-TT-1	8.40x19.00	159.60	89.60	382.84	561
W-A-TT-2	8.20x19.00	155.80	88.10	393.57	565
W-B-TT-1	5.00x13.10	65.50	36.50	419.30	557
W-B-TT-2	4.70x13.10	61.57	34.40	428.26	559

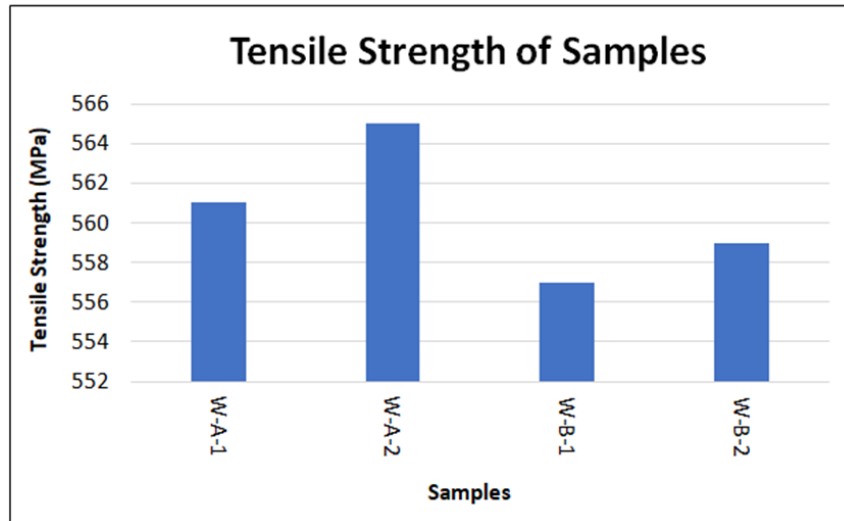


Figure 4. Tensile strength of W-A-1, W-A-2, W-B-1, W-B-2

An analysis of the graph in Figure 4 indicates that the tensile strength of the W-A coded weld samples exceeds that of the W-B coded weld samples. The maximum tensile strength recorded was 565 MPa, observed in the W-A-2 coded weld sample, while the minimum was 557 MPa, recorded in the W-B-1 coded weld sample. Both tensile test results in each series produced very close results and the difference in results is insignificant ($< 0.1\%$), making the third test unnecessary. When all mechanical properties are evaluated collectively, irrespective of material thickness, it has been deduced that the application of welding might have created residual stress on the joint and its surroundings, which has a detrimental effect on its strength properties and results in a brittle failure. It has been established that residual stresses occur during the welding process, due to a reduction in percent elongation, an increase in fracture toughness in the welded area and the heat affected zone (HAZ). In samples that have undergone heat treatment, it has been determined that the application of welding increases the yield strength and tensile strength, as well as the percentage elongation [16, 17]. Furthermore, the effects of residual stress have been found to decrease with an increase in impact toughness. The findings of this study demonstrate that, while the stress relief process following welding does not fully restore the properties of the material prior to welding application, it does restore a substantial portion of these properties and enhances its strength, thereby confirming its necessity.

3.2. Hardness Test Results

Hardness values were taken in the W-A coded welding process, the W-B coded welding process at 15 points along the line for the cover pass and at 15 points along the line for the root pass. Hardness measurements were made according to ASTM E92-23 standard. Hardness distribution is a measure of line hardness and example of line hardness measurement is shown in Figure 5. Minimum recommended range for Vickers hardness measurement is shown in Figure 6. Hardness distribution values of welding processes coded W-A, W-B are shown in Figure 7a-b.

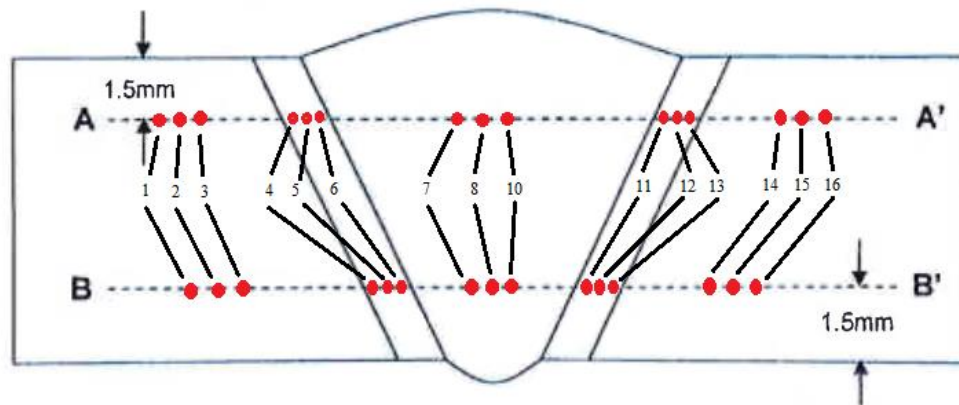


Figure 5. Example of line hardness measurement.

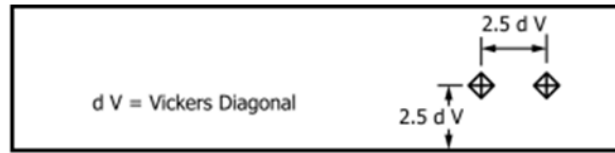


Figure 6. Minimum recommended range for Vickers hardness measurement.

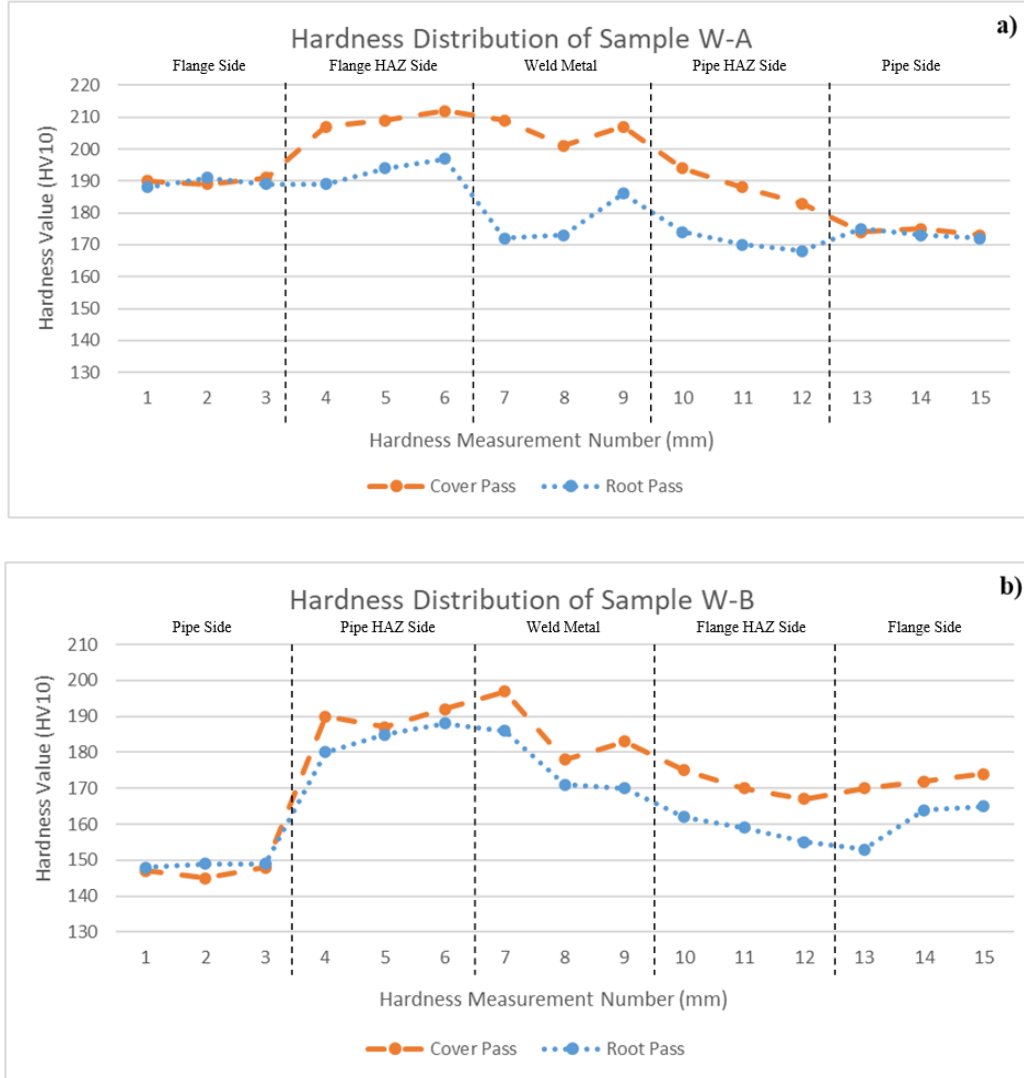


Figure 7. Line Hardness distribution for a) the W-A coded welding process b) the W-B coded welding process.

Figure 7a presents a graphical representation of the hardness values of the cap pass and root pass for the W-A welding process. It can be observed that the hardness value of the cap pass in the weld filler metal is higher than that of the root pass. The highest recorded hardness value is 212HV, which is observed in the HAZ (Heat Affected Zone) of cap pass. In the root pass, the lowest recorded hardness value is 168HV, which was observed in the A333 Gr6 base metal region. Figure 7b presents the hardness values of the cap pass and root pass for the W-B welding process. It can be observed that the hardness value of the root pass in HAZ is nearly identical to that of the cap pass. The highest recorded hardness value is 197HV, which is observed in the cap pass weld metal region. The lowest hardness value observed in the A333 Gr6 base metal region is 145 HV. Upon examination of the hardness graphs, it becomes evident that the transitions of local hardness values are softer in the heat-treated sample, with the hardness values of the root and cap pass being relatively similar. In contrast, in the unheat-treated sample, local hardness transitions are observed to be harder, with a notable difference in hardness values between the root and cap passes, which can be traced back to residual stresses at root and cover passes, the latter is tensile, and the former is compressive, respectively [14]. These stresses are relieved when heat treatment is applied and the difference between the hardness values is smaller whereas non heat-treated specimens contain such differences in stress and hence difference in hardness

values are larger [18, 19]. The results of the hardness analysis indicated that the observed variations in strain and softening within the welds can be attributed to the processes of recovery and recrystallization. These two phenomena were identified as the predominant factors influencing the alterations in hardness within both the heat-affected zones (HAZ) and the base metal regions during the process of multilayer welding [20].

3.3. Charpy V Notch Impact Test Results

The notch impact test results of the W-A and W-B coded welded samples are shown in Table 9. 3 impact test values were obtained from each sample and the average impact toughness values are presented. The distribution of the average impact toughness values of the W-A and W-B coded welded samples is shown in Figure 6.

Table 9. Charpy V Notch Tests results on samples obtained from the welding process coded W-A and W-B.

Specimen No	Notch Location	Dimension (mm)	Test Temp. (°C)	Impact Toughness Value (J)			Average (J)
W-A-NT-1	F+5mm (Pipe Side)	10x10x2V	-46	220	230	182	211
W-A-NT-2	F+2mm (Pipe Side)	10x10x2V	-46	62	138	28	76
W-A-NT-3	Weld Centre Line	10x10x2V	-46	92	90	104	95
W-A-NT-4	F+2mm (Flange Side)	10x10x2V	-46	170	150	184	168
W-A-NT-5	F+5mm (Flange Side)	10x10x2V	-46	170	198	158	175
W-B-NT-1	F+5mm (Pipe Side)	10x4x2V	-53	84	90	80	85
W-B-NT-2	F+2mm (Pipe Side)	10x4x2V	-53	84	66	14	55
W-B-NT-3	Weld Centre Line	10x4x2V	-53	42	40	36	39
W-B-NT-4	F+2mm (Flange Side)	10x4x2V	-53	32	58	32	41
W-B-NT-5	F+5mm (Flange Side)	10x4x2V	-53	32	38	24	31

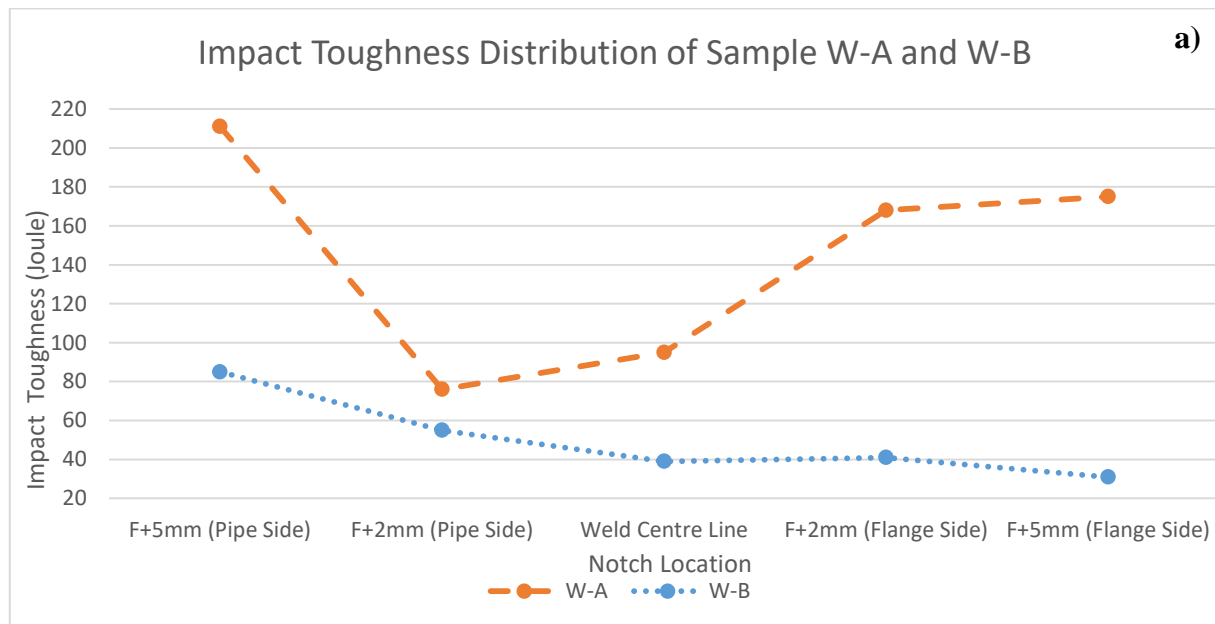


Figure 8. Impact toughness distribution for the W-A and W-B coded welding processes.

When Figure 8 is examined, it can be seen that the impact toughness of the W-A coded weld samples is higher than the impact toughness of the W-B coded weld samples. The lowest average impact toughness

value belongs to the W-B coded weld sample, which is 31 J. The highest average impact toughness value belongs to the W-A coded weld sample, which is 211 J. This situation is due to the increase in toughness due to heat treatment. Metallic materials become brittle below a certain temperature (transition temperature) and the impact toughness of the material decreases significantly. Above this temperature the material becomes ductile and thus, the crack formation and propagation become more difficult and the impact toughness increases as with finer grain increasing the impact toughness.

In steels, carbon and other alloying elements affect the impact toughness at a certain temperature as well as the transition temperature. As the carbon content in steels increases, ductility decreases and the transition temperature increases. Other alloying elements also affect the impact resistance and transition temperature. For example, the addition of Mn to a steel containing Fe-%0.05 C reduces the transition temperature. While the transition temperature of an alloy containing Fe-%0.05 C is 70 °C, it decreases to 10 °C with the addition of 0.5% Mn, to -20 °C with the addition of 1% Mn, and to a value lower than -60 °C with the addition of 2% Mn. The transition temperature decreases with the increase in the Mn/C ratio. In practice, Mn content above 1.4% and 2% C provides the desired tensile properties. A nickel content of up to 2% effectively reduces the transition temperature. The silicon content above 0.25% increases the transition temperature. Molybdenum, like carbon, rapidly increases the transition temperature. For high purity iron, oxygen content above 0.003% causes intergranular fracture and low energy absorption. When oxygen content increases from 0.001% to 0.057%, the transition temperature increases from -15 °C to 340 °C. This also reveals the importance of deoxidation. In low carbon steels, if the normalization process is carried out at a very high temperature after hot rolling, the transition temperature decreases. The cooling rate and deoxidation after normalization should be taken into consideration. Cooling in air and deoxidation with aluminum further reduce the transition temperature. Coarse grained steels have low impact resistance and high ductile-brittle transition temperatures [13, 21, 22].

3.4. Macro Image Results

Macro images of welding processes coded W-A, W-B are shown in Figure 9a-b.

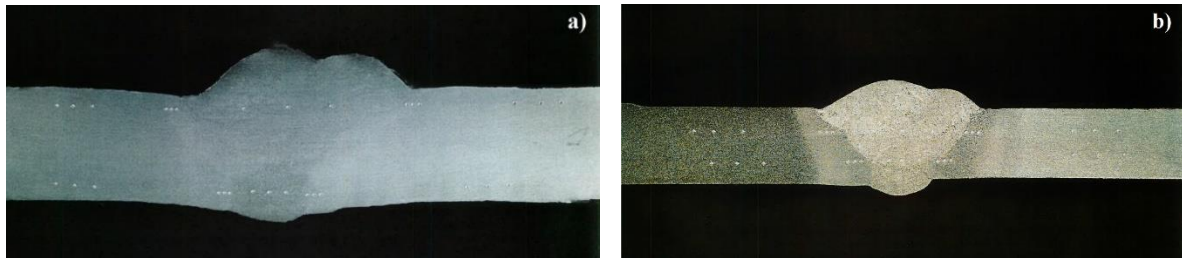


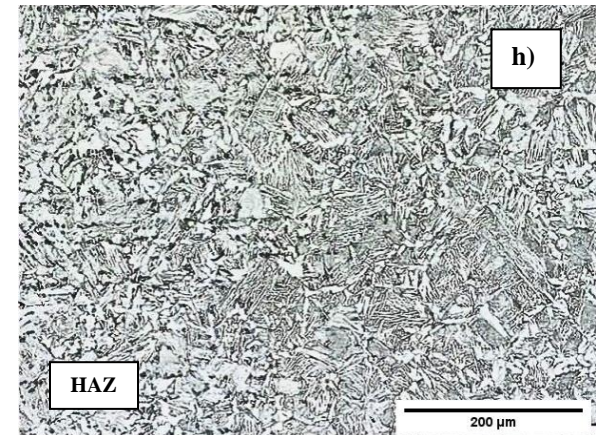
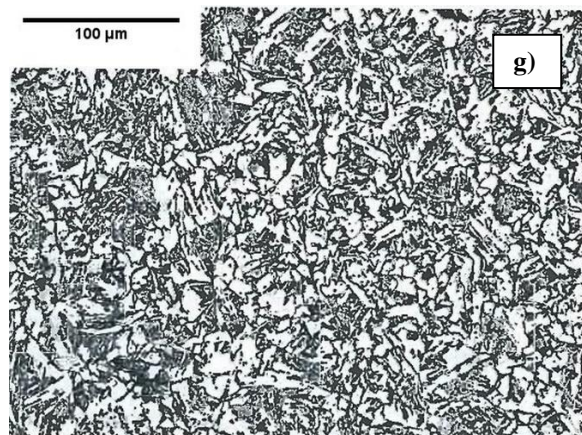
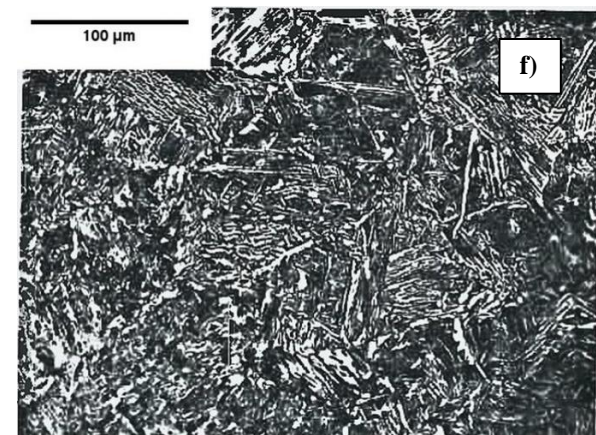
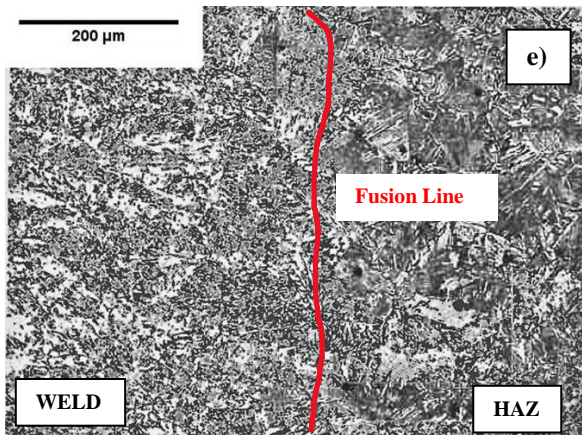
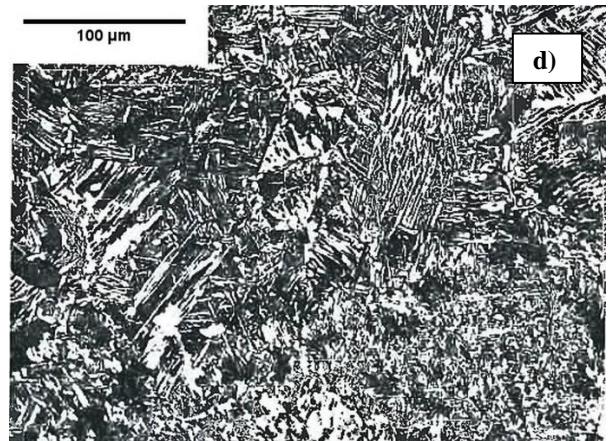
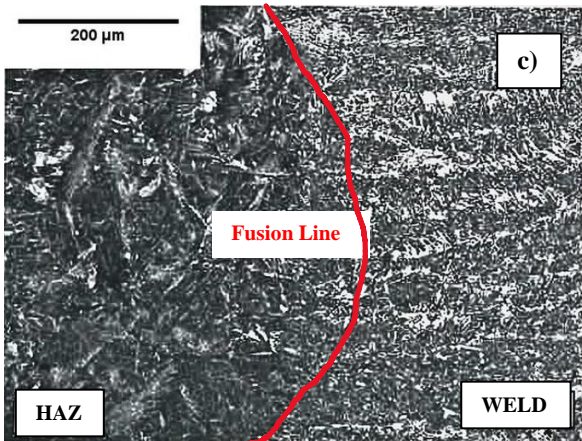
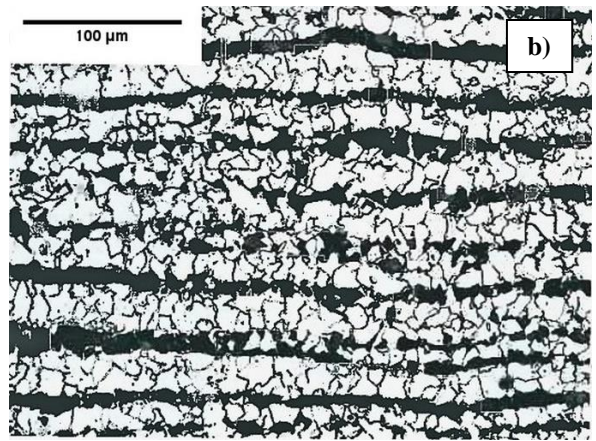
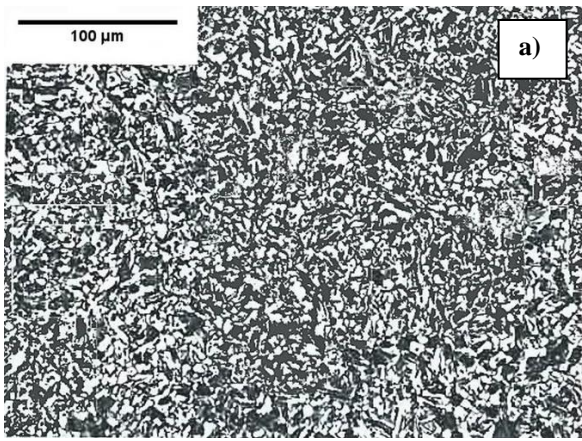
Figure 9. The macro image of a) the W-A coded welding process b) the W-B coded welding process.

When the macro images of the samples are examined, it is clearly seen that the heat treatment reduces the HAZ in the welded sample with code W-A in Figure 9a. In the welded sample with code W-B in Figure 9b, the HAZ region is larger because no heat treatment was applied after welding and also because of the lower base metal thickness.

A thorough examination of the macrostructure images reveals the absence of weld pits, cracks, voids, inadequate fusion, low penetration, slag residues and burning grooves in the weld area. This observation indicates that the welding parameters have been appropriately selected. Additionally, it is observed that weld sag and errors resulting from excessive welding amperage do not occur. The macrostructure photographs demonstrate the distinction between the two passes and the clear delineation of the weld area, HAZ, and base material regions. The orientation of grains in the weld area is observed to be aligned with the heat flow, and the HAZ region is found to be wide, a consequence of the high heat input in both passes and the slow welding speed.

3.5. Microstructural Image Results

Microstructural images of weld metals and their subzones obtained from different welding processes are shown in Figure 10a-j.



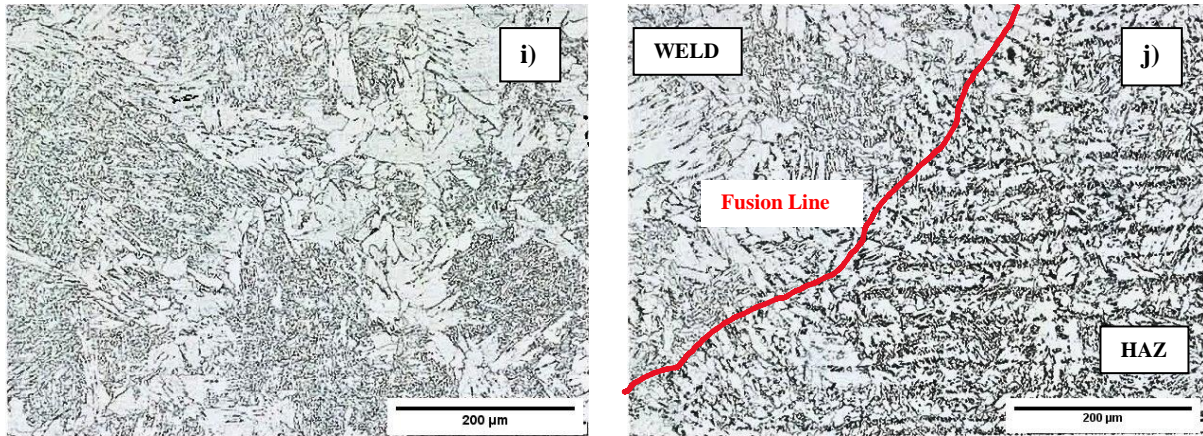


Figure 10. Microstructural images of a) A350LF-2 Base Metal b) A 333 Gr.6 Base Metal c) A350LF-2 Fusion Line d) A350LF-2 Fusion Line (200x magnification) e) A 333 Gr.6 Fusion Line f) A 333 Gr.6 Fusion Line (200x magnification) g) Weld Metal h) PWHT HAZ i) PWHT Weld Metal j) PWHT Fusion Line

The microstructure in Figure 10a shows that the A350LF-2 base metal has a fine-grained structure. Very fine ferrite grain along with small amounts of ferrite-cementite aggregates between subgrains can be observed. A heat treatment followed by high deformation ratio may result in such microstructures in low carbon steels. As seen in the microstructure in Figure 10b, the A 333 Gr.6 base metal consists of comparatively larger ferrite grains along with banding structures which are remnants of rolling during the hot deformation process, indicating that the rolling process took place at temperatures where microsegregation of carbon or cementite structure occur. A hypoeutectoid ferrite forms due to carbon redistribution prior to phase transformation i.e. A3 to A1 and it is followed by carbon concentration imbalance during hot rolling, which is also helped by recrystallization of new nuclei [23, 24]. Figure 10c shows that the right side of the A350LF-2 fusion line is the weld metal and the left side is the HAZ (Heat Affected Zone). The weld metal contains very high amount of fine-grains and acicular ferrite structures which are visible in the weld metal region, whilst structures similar to the Widmanstatten ferrite structure are visible in the heat-affected zone (HAZ). The grain boundaries are decorated with grain boundary ferrite with very small amounts of ferrite plates emanating from proeutectoid ferrite subgrains. However, Figure 10d shows very different microstructure and it presents dominantly ferrite side plates with fine cementite films in between them, i.e. similar to Bainite structures but it is not fully conclusive with the 200x magnification of the A350LF-2 fusion line image. In Figure 10e, the right side of the A333 Gr.6 fusion line is identified as the HAZ, while the left side corresponds to the weld metal. The weld metal consists of fine acicular ferrite structure with slightly increased number of recovered proeutectoid ferrite or grain boundary ferrite. The HAZ region exhibits grain coarsening with increased level of widmanstatten ferrite protruding into the grain interior and there are more over recovered coarsened ferrite subgrains inside thegrains and along the grain boundary. In Figure 10f, the 200x magnification of the A333 Gr.6 fusion line reveals the presence of mixture of coarse high temperature, that is, upper bainitic structures and ferrite cementite side plates with acicular structures between the ferrite-cementiteregions as it is difficult to see fine pearlite at this carbon level. In Figure 10g, an increase in fine ferrite grain structures are observed in the weld metal region, indicating the presence of small amount of acicular sturctures which are smaller in size and length. Such small grains are possible to produce when weld metal has higher amounts of Mn and or Si as they are responsible to produce effect similar to carbonto lesser effect, that is, lower the critical cooling rate and hence refine the grain structure and its interior with possibly increasing the amount of fine oxides [25]. Figure 10h reveals the presence of carbide formations between ferrite grain boundaries on the weld filler metal side of the heat-treated HAZ (left side). On the right side, the growth and coarsening of the Bainite structures is evident with acicular ferrite. Plated structures bear a resemblance to ferrite side plates and irregular form of subgrains which are possibly product of coarsening as evidenced by the microstructure analysis depicted in Figure 10i. It is observed that the ferrite side plate structures have undergone a coarsening process in the heat-treated weld metal. In comparison, the Ferrite structures appear to have experienced a reduction in thickness. Upon examining the microstructure in Figure 10j, it is evident that the Bainite and acicular structures have undergone a coarsening process on the weld filler metal side of the heat-treated Fusion Line (left side). Highly recovered coarse ferrite appears to form on the HAZ region side (right side).

4. CONCLUSION

The present study investigates the effect of heat treatment on the mechanical properties of materials, and the changes that occur after stress relief, in welds made with the same materials, the same electrodes, and the same welding methods, but with different thicknesses. The following findings were obtained:

- When tensile samples are examined, the maximum tensile strengths of the samples subjected to heat treatment with code W-A are higher than those of the samples without heat treatment with code W-B. The main reasons for this can be said to be the elimination of residual stresses after heat treatment and the reduction of grain structures of the normalized material.
- The samples demonstrated successful performance in the 180° bending test, with no observable breakage, tearing, or visible discontinuity or defect. The positive outcomes observed in the 180° three-point bending test on the samples indicate that the welding process was executed correctly and that the selected filler metals were appropriate for the material combination utilised in this process.
- The hardness value of the coke pass weld filler metal of the sample subjected to heat treatment with code W-A is similar to the hardness value of the A333 Gr6 base metal. This confirms that the heat treatment is smooth and homogeneous.
- When the effect of heat treatment on the material is examined, it is seen that the average fracture toughness of the W-A sample is much higher than the W-B sample. The reason for this can be said to be the reduction of grain sizes due to the elimination of residual stresses caused by heat treatment.
- A thorough examination of the macrostructure photographs reveals that no weld pits have been formed. Furthermore, no cracks, voids, lack of fusion, low penetration, slag residues or burning grooves have been observed in the weld area. Consequently, it can be concluded that the welding parameters have been selected at appropriate values.
- In the W-A welding process, which is performed with a material approximately twice as thick, the material thickness increases the cooling rate and encourages the hardening tendency, so this situation is prevented by applying heat treatment after welding, thus eliminating the stresses.
- The data demonstrate that, although the stress relief process after welding does not completely restore the properties of the material before welding application, it restores a significant portion of these properties and increases the strength of the material, thus proving its necessity.
- A study of the microstructures of non-heat-treated welding processes reveals the presence of ferrite, pearlite, acicular ferrite, Widmanstätten ferrite, and fine bainite structures. Conversely, the microstructures of heat-treated welding processes exhibit ferrite, pearlite, lamellar pearlite, coarse bainite, and acicular ferrite structures.

REFERENCES

- [1] J.M. Tanzosh, Chapter A3: Piping Materials, in Piping Handbook, New York, McGraw-Hill, 2000.
- [2] Norsok Standard, M-001 Material Selection, Norwegian Petroleum Industry, Norway, 2004.
- [3] M. Stipanicev, F. Turcu, L. Esnault, O. Rosas, R. Basseguy, M. Szttyler, I.B. Beech, Corrosion of carbon steel by bacteria from North Sea offshore seawater injection systems: Laboratory investigation, Bioelectrochemistry 97, (2013), 76-88. <https://doi.org/10.1016/j.bioelechem.2013.09.006>
- [4] S. Papavinasam, Chapter 3 – Materials, Corrosion Control in the Oil and Gas Industry, 2014.
- [5] M.F. Ashby, Materials Selection in Mechanical Design, Burlington: Elsevier Publisher, 2005.
- [6] A.J. Bryhan, W. Troyer, Weldability of a low carbon Mo-Nb X-70 pipeline steel, Welding Research, 1980.
- [7] P. Smith, Piping Materials Selection and Applications, Burlington: Gulf Professional Publishing, 2005.
- [8] American Society for Testing and Materials (ASTM), ASTM A333: Standard specification for seamless and welded steel pipe for low-temperature service, American Society for Testing and Materials (ASTM), Washington, 2013.
- [9] Z. Wang, Y. Li, C. Chang, Application of automatic TIG welding for Yamal LNG process piping fabrication International Journal of Oil, Gas and Coal Engineering 6, (2018), 44-49. <https://doi.org/10.11648/j.ogce.20180604.11>
- [10] A.B. Nissan, K.C. Baker, Determination of the cause of low temperature charpy toughness values in ASTM A350 LF2 Flanges, Proceedings of the 28th ASM Heat Treating Society Conference, USA, 2015: pp. 342-349.
- [11] P.K. Ghosh, P.K. Singh, K.K. Vaze, H.S. Kushwaha, Characterisation of pipe welds and HAZ in primary heat transport system piping of pressurised heavy water reactors, Science and Technology of Welding and Joining, 9 (2004) 200-208.
- [12] M.E. Efsan, S. Kesahvanveraragu, J. Emerson, Microstructural characterization and hardness properties of A333 grade 6 low carbon steel in offshore platform pipelines, Journal of Advanced Research in Materials Science 2 (2014) 1-9.

- [13] E.S. Kayalı, C. Ensari, F. Dikeç, Metalik malzemelerin mekanik deneyleri, İTÜ Kimya-Metalurji Fakültesi, Ofset Atölyesi, İstanbul, 1996.
- [14] S. Fowler, A. Toumpis, A. Galloway, Fatigue and bending behaviour of friction stir welded DH36 steel, *Int J Adv Manuf Technol* 84, (2016), 2659-2669.
- [15] T.L. Dickerson, J. Przydatek, Fatigue of friction stir welds in aluminium alloys that contain root flaws, *Int J Fatigue* 25, (2003), 1399–1409.
- [16] I.V. Vlasov, A.I. Gordienko, V. M. Semenchuk, Heat treatment effect on structure and mechanical properties of gas metal arc-welded pearlitic steel, *Russ Phys J*, 67, (2024), 1590-1598. <https://doi.org/10.1007/s11182-024-03286-y>
- [17] X. Wang, D. Wang, L. Dai, C. Deng, C. Li, Y. Wang, K. Shen, Effect of post-weld heat treatment on microstructure and fracture toughness of X80 pipeline steel welded joint, *Materials*, 15(19), (2022), 6646.
- [18] K.A.M.B. Gonçalves, G.L. de Faria, R.H.M. de Siqueira, T.R. de Oliveira, M.S.F. de Lima, Heat treatment effects on the hardness and wear behavior of laser-welded AISI40 martensitic steel plates, *Int J Adv Manuf Technol* 114, (2021), 1155-1163.
- [19] C. Köse, R. Kaçar, The effect of preheat & post weld heat treatment on the laser weldability of AISI 420 martensitic stainless steel, *Mater Design* 64, (2014), 221-226.
- [20] L. Yu, K. Nishimoto, H. Hirata, K. Saida, Hardness prediction of the heat-affected zone in multilayer welded SUS316 stainless steel based on dislocation density change behavior, *Metall Mater Trans A*, 55, (2024) 1788-1803.
- [21] L.E. Svenson, B. Gretoft, Microstructure and impact toughness of C Mn weld metals, *Welding Journal*, (1990) 454-461.
- [22] A. Ilić, I. Miletić, R.R. Nikolić, V. Marjanović, R. Ulewicz, B. Stojanović, L. Ivanović, Analysis of influence of the welding procedure on Impact Toughness of welded joints of the High-Strength Low-Alloyed Steels, *Applied Sciences* 10(7), (2020), 2205.
- [23] C.F. Jaczak, D.J. Girardi, E.S. Rowland, On banding in steel, *Transactions of the ASM* 48, (1956), 279-305.
- [24] P.G. Bastien, The mechanism of formation of banded structures. *Journal of the Iron and Steel Institute*, 187, (1957), 281-291.
- [25] G. Evans, Effect of Si on the microstructure and properties of C-Mn all weld metal deposits, *Metal Construction* (1986).